

Ion-molecule reactions and ion energies in a CF₄ discharge

B. L. Peko,* I. V. Dyakov, and R. L. Champion[†]

Department of Physics, College of William and Mary, Williamsburg, Virginia 23187

M. V. V. S. Rao[‡] and J. K. Olthoff[§]

Electricity Division, Electronics and Electrical Engineering Laboratory, National Institute of Standards and Technology, Gaithersburg, Maryland 20899-8113

(Received 11 March 1999)

Absolute cross sections have been measured for reactants typically found in carbon tetrafluoride (CF₄) discharges for collision energies below a few hundred electron volts. The reactions investigated include collision-induced dissociation and dissociative electron transfer reactions for CF₃⁺ and F⁺ colliding with CF₄, and collisional electron detachment for F⁻ colliding with CF₄. Also presented are measurements of energies and relative intensities of ions generated in dc Townsend CF₄ discharges with E/N values ranging from 4×10^{-18} V m² to 25×10^{-18} V m² [4 to 25 kTd]. Ion energy and ion intensity data for the Townsend discharges are analyzed in light of the measured cross sections. [S1063-651X(99)05212-5]

PACS number(s): 52.20.Hv, 52.80.Dy, 34.50.-s

I. INTRODUCTION

Quantitative knowledge of ion-molecule reactions is essential for understanding the production and transport of ions in many electrical discharges. Recent reports [1] and articles [2] have strongly indicated the need for data on ion-molecule reactions for species related to the gases used in the semiconductor industry. This need is driven primarily because of the essential role that ion bombardment plays in various etching and deposition processes, and the desire to develop predictive models for these processes. Ion-molecule reactions may also play a significant role in newly developed techniques for the destruction of waste gases from plasma reactors, and detailed modeling of these methods may produce more efficient procedures.

The majority of ion-molecule data found in the literature were derived from atmospheric oriented research. Few data are available for plasma processing gases. Carbon tetrafluoride (CF₄), for example, is one of the most commonly used plasma processing gases, but no ion-molecule cross sections are available in the literature. Consequently, plasma models [3-6] for CF₄ systems either do not include potentially important ion-molecule reactions, or use estimates for cross section values.

In order to provide some of the essential ion-molecule interaction data that are needed for such modeling, and in order to enhance the understanding of ion transport in simple CF₄ discharges, we present and relate the results of two experiments. In the first part of this paper, we present absolute cross section measurements for ion-molecule reactions involving positive and negative ions typically found in dis-

charges containing CF₄. The reactions investigated here include dissociative charge transfer collisions of F⁺ and CF₃⁺ with CF₄, collision-induced dissociation for CF₃⁺ colliding with CF₄, and collisional electron detachment for F⁻ colliding with CF₄. Cross sections have been determined for relative collision energies ranging from 20 to about 400 eV for F⁺ and CF₃⁺ and from 2 to 80 eV for F⁻.

In the second portion of this paper we present measurements of relative intensities and energies of ions generated in a dc Townsend discharge in CF₄. This simple discharge was chosen for study because in many ways it emulates the sheath region of more complex discharges, and it lends itself to modeling efforts [7]. Measurements were made for discharges with electric field-to-gas density ratios E/N ranging from 4×10^{-18} to 25×10^{-18} V m² [4 to 25 kTd], which are comparable to those found in the sheaths of some plasma processing discharges. The cross sections presented in the first part of the paper are used to provide an interpretation of the primary features of the Townsend-discharge ion data. However, it is clear that a complete understanding of the ion kinetics in even this simple discharge requires additional cross section data and sophisticated modeling.

II. EXPERIMENT

A. Ion-molecule cross section experiment

In the first experiment, absolute cross sections were determined using complementary electrostatic trapping and crossed beam techniques which have been described in detail previously [8,9]. Briefly, the primary ions F⁺, CF₃⁺, or F⁻, are formed in a low pressure (~1.3 Pa) arc discharge source using a mixture of 10% CF₄+90% Ar as the discharge gas. The signal intensities of other ions from the source, such as CF⁺ and CF₂⁺ were too small to allow cross section measurements. After extraction and mass analysis, the primary ions are focused into an electrostatic trapping cell for direct measurement of absolute cross sections for collision induced dissociation (CID), the sum of all dissociation

*Present address: Physics department, University of Denver, Denver, CO 80208-2238.

[†]Electronic address: champion@physics.wm.edu

[‡]Present address: NASA/Ames Research Center, Moffet Field, CA 94035-1000.

[§]Electronic address: james.olthoff@nist.gov

tive charge transfer (DCT) reaction channels, or electron detachment (ED). The scattering region of the cylindrically symmetric cell consists of a collision chamber (scattering path ~ 46 mm), detection plates, three 90% transparent parallel grids, and a Faraday collector. The target gas pressure is maintained at 0.05 Pa. The range of ion energies over which accurate CID and DCT cross section measurements can be made is from 20 to 400 eV, with the lower energy limit determined by large angle elastic and inelastic scattering of the primary ion beam. Measurement of ED cross sections extends to much lower energies (approximately 2 eV) as the detached electrons are confined by magnetic trapping.

By varying the retarding voltages on the grids, one can effectively isolate slow product ions associated with various dissociative charge transfer channels collectively, as well as certain more energetic CID products. By applying a small axial magnetic field (~ 12 G) to the collision chamber, electrons resulting from detachment or target ionization are confined to a small radius of gyration, allowing for their separation and detection and hence determination of total cross sections for electron detachment from F^- , or target ionization in the case of positive primary ions. In order to ascertain cross sections for each DCT channel uniquely, a crossed beam arrangement is implemented. Here the primary beam passes resonantly between two curved plates of a cylindrical capacitor (mean radius of 76 mm) and intersects orthogonally with the target gas injected from above. The slow positive product ions are forced through an aperture in the inner wall of the capacitor and subsequently focused into a quadrupole mass analyzer. Product ion intensities are measured in counting mode using a continuous dynode electron multiplier operated so that its detection efficiency is close to unity for both singly and doubly ionized products. Branching ratios for slow product ions are then determined and combined with the trapping cell results to determine cross sections for specific DCT processes. Uncertainties for the CID measurements are estimated to be within $\pm 15\%$, while those for DCT measurements are within $\pm 20\%$. To provide an additional check of the present experimental method, cross sections for DCT producing CF_3^+ and CF_2^+ arising from collisions of Ar^+ with CF_4 were measured and compared to previous results of Fisher, Weber, and Armentrout [10]. These latter experiments employed a guided beam technique in which the primary ion beam was injected into an rf octupole ion beam guide and collision cell, allowing all slow charged products to be effectively collected. Our results agreed with those of Fisher, Weber and Armentrout to within 10% over the range of energies common to both experiments, viz., 25 to 50 eV.

B. Townsend discharge experiment

In the second experiment, the relative intensities and energies of ions produced in dc Townsend discharges in CF_4 are measured. The experimental apparatus used here is essentially the same as used previously in our studies of Townsend discharges in rare gases [11] and oxygen [12]. Briefly, the discharge cell consists of two flat, parallel, 11-cm-diam. stainless steel electrodes separated by a 2-cm gap and surrounded by a cylindrical quartz tube. The discharge is generated by introducing a gas between the plates, and then

biasing the upper electrode either positively or negatively in order to sample positive or negative ions, respectively, at the grounded electrode. The pressure in the discharge ranges from approximately 5 to 20 Pa.

Ions from the discharge pass through a 0.1-mm sampling orifice in the grounded electrode and enter a differentially pumped, 45° electrostatic ion-energy analyzer and quadrupole mass spectrometer system, which has been described previously [11–13]. The resolution of the mass spectrometer was approximately 1 u (amu), and the resolution of the electrostatic energy analyzer was maintained at 4 eV, independent of the mass and energy of the ion. The kinetic energy distributions of ions striking the grounded electrode are measured by setting the quadrupole to transmit ions of a particular mass, and then scanning the potential of the energy analyzer. As discussed in Refs. [11] and [12], the resulting distribution function is an ion-flux energy distribution, i.e., the number of ions per second with energy between ϵ and $\epsilon + d\epsilon$ that strike a particular area of the grounded electrode [14].

In a Townsend discharge the currents are sufficiently low ($< 100 \mu A$) such that space charge effects are negligible, i.e., space charge does not significantly affect the applied electric field between the electrodes. Thus assuming the ions experience many collisions as they travel across the gas, the energies of the ions will be dependent only upon the ratio of the electric field strength to the gas number density E/N . The electric field strength E in the discharge gap is assumed to be given by V_d/d , where d is the interelectrode gap spacing (2 cm) and V_d is the voltage drop across the gap. The gas density N is determined from the gas pressure in the gap region as measured by a capacitive manometer (baratron). The combined errors of these measurements indicates that the uncertainty in the measured E/N of a discharge is $\pm 3\%$.

III. EXPERIMENTAL RESULTS

A. Ion-molecule reactions

A list of observed reaction channels and their respective endothermicities for ground state reactants and products is given in Table I, where the endothermicities are expressed in eV. Underlined products, which are fragments of the primary ions, have roughly the same laboratory velocity as the reactant ion. Therefore CF_2^+ formed from collision induced dissociation of CF_3^+ will have $\frac{50}{69}$ of the kinetic energy of the primary ion. The laboratory kinetic energy of all other charged products will be small compared to that of the projectile. Shown in bold are the observed product ions or free electrons.

1. $F^+ + CF_4$

A mass spectrum illustrating the DCT products for collisions of F^+ with CF_4 for relative collision energy ϵ of 66 eV is given in Fig. 1. The figure clearly illustrates the remarkable variety of chemically reactive species—including doubly charged products—arising from these reactants. As mentioned earlier, the spectra are acquired in a pulse counting mode which does not preferentially detect doubly charged ions. Thus the relative intensities for CF_2^{2+} and CF_3^{2+} are scaled in the same manner as is done for CF^+ , etc. The

TABLE I. Reactants and products related to measurements reported herein. The endothermicities are given in eV, the products of CID are indicated in italics, the underlined products have roughly the same laboratory velocity as the reaction ion, and the observed product ions or electrons are shown in bold.

Reaction Number	Reactants	Products	Endothermicity ^a (eV)
1	$F^+ + CF_4$	$CF_3^+ + F + F$	+2.7
2		$CF_2^+ + F_2 + F$	-1.9
3		$CF^+ + F_2 + F + F$	-4.7
4		$C^+ + 2F_2 + F$	-10.8
5		$F^+ + CF_3 + F$	< -10.8
6		$CF_3^{++} + F + F^-$	-21
7		$CF_2^{++} + F_2 + F^-$	-21.1
8	$CF_3^+ + CF_4$	$CF_3^+ + F + CF_3$	-5.7
9		$CF_2^+ + F_2 + CF_3$	-10.3
10		$CF^+ + F + F_2 + CF_3$	-13.1
11		$C^+ + 2F_2 + CF_3$	-19.2
12		$CF_2^+ + F + CF_4$	-6.2
13		$CF^+ + F_2 + CF_4$	-7.4
14		$F^+ + CF_2 + CF_4$	-12.3
15		$C^+ + F + F_2 + CF_4$	-15.1
16	$F^- + CF_4$	$e + CF_4 + F$	-3.4

^aEndothermicities listed were derived from information in Ref. [15], and references cited therein. Positive values of endothermicity indicate an exothermic reaction.

endothermicities shown in Table I are based on the assumption of ground state reactants and products and, for the doubly charged product ions, that F^- is a product rather than $e^- + F$. The cross section for producing electrons σ_e , could also be measured with the present experimental apparatus and it was found that $\sigma_e < 0.05 \text{ \AA}^2$ (the lower detection limit of the apparatus) for the energy range of the experiments (20 eV $< \epsilon < 350$ eV), thus supporting the above assumption that anion products are associated with doubly charged products.

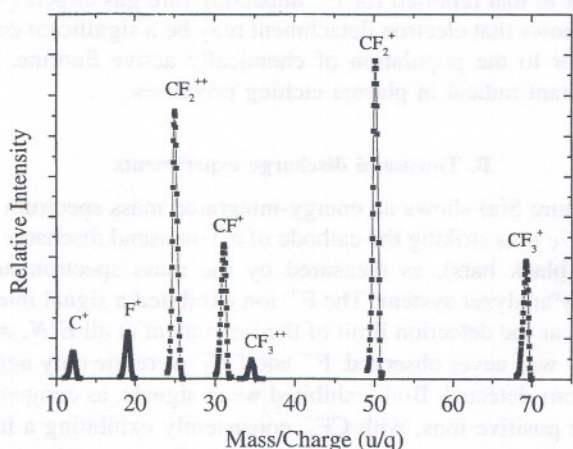


FIG. 1. Mass spectrum for ions produced from collisions of F^+ with CF_4 for $\epsilon = 66$ eV.

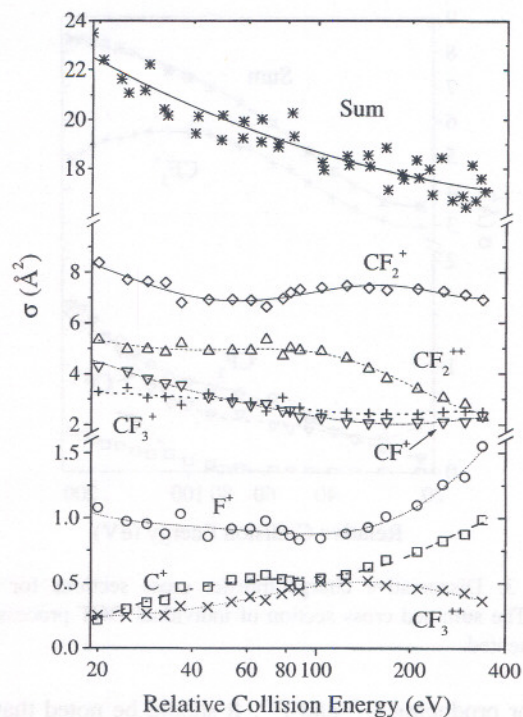


FIG. 2. Absolute cross sections for individual DCT reaction channels presented as a function of relative collision energy for the reactants F^+ and CF_4 . The total DCT cross section is also shown.

Figure 2 illustrates the summed cross section for all DCT processes as a function of the relative collision energy, along with those for its constituent channels (reactions 1–7 in Table I). Unexpected are the small values for producing CF_3^+ , despite the fact that this process is exothermic by 2.7 eV owing to the large ionization potential for F.

Perhaps the most interesting result is the substantial cross section for producing CF_2^{++} , illustrating an efficient process for the conversion of F^+ to F^- . This reaction exhibits an unexpectedly large cross section with a surprisingly low threshold energy. Doubly charged CF_2^{++} is apparently produced for ion-collision energies below the ground state energetic threshold of ~ 21 eV, a value derived from electron-impact appearance potential (AP) measurements [16] that assume the process $e + CF_4 \rightarrow CF_2^{++} + F_2 + 3e$. If the AP products were actually $F_2^- + 2e$, the reaction would be some 3 eV less endothermic, i.e., 18 eV.

The detection of CF_2^{++} for low collision energies suggests the possibility that the primary ion beam is comprised of ground and metastable states of F^+ , most probably $F^+(^1D)$ and $F^+(^1S)$, 2.59 and 5.56 eV above ground state $F^+(^3P)$, respectively. A multiple state F^+ beam is not uncommon when the ion is formed in an electron impact ionization source with an Ar: CF_4 mixture as the source gas and electron energies exceeding 50 eV [17,18]. In the present experiments the kinetic energy of the electrons in the positive ion source was 100 eV and could not be lowered by more than about 10 eV due to a substantial decrease in F^+ ion beam current, an observation in agreement with the results of Lin *et al.* [18]. Increasing the source gas pressure to collisionally deexcite metastable F^+ ions is probably ineffective as singlet to triplet transitions would not be expected to have large cross sections. It is interesting to note that, although small, the cross sections for production of CF_3^{++} are still comparable with

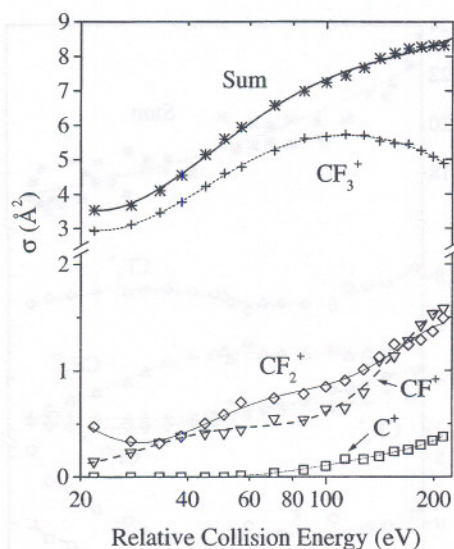


FIG. 3. Dissociative charge transfer cross sections for $\text{CF}_3^+ + \text{CF}_4$. The summed cross section of individual DCT processes is also presented.

those for producing C^+ and F^+ . It should be noted that the endothermicity for production of CF_3^{++} given in Table I was also based on AP measurements and the assumption that $e + \text{CF}_4 \rightarrow \text{CF}_3^{++} + \text{F} + 3e$.

2. $\text{CF}_3^+ + \text{CF}_4$

The number of DCT product channels for these reactants (reactions 8–11 in Table I) is considerably fewer than what is observed for the F^+ projectile. Specifically, no doubly charged ions or F^+ is observed for $\text{CF}_3^+ + \text{CF}_4$. The total cross section for DCT is given in Fig. 3 along with the individual cross sections for the production of the principal DCT products. The energy levels for these product channels are given in Table I, where again ground state reactants and products are assumed. The magnitudes of the cross sections decrease substantially as the endothermicity of the reaction increases.

Cross sections for collision induced dissociation (CID) were also measured for these reactants for collision energies, $30 \text{ eV} < \varepsilon < 230 \text{ eV}$, but are not shown here. The three CID channels (reactions 12–15 in Table I) producing C^+ and F^+

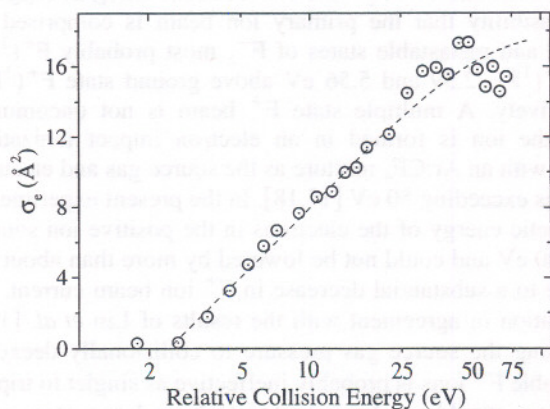


FIG. 4. Electron detachment cross section for collisions of F^- with CF_4 .

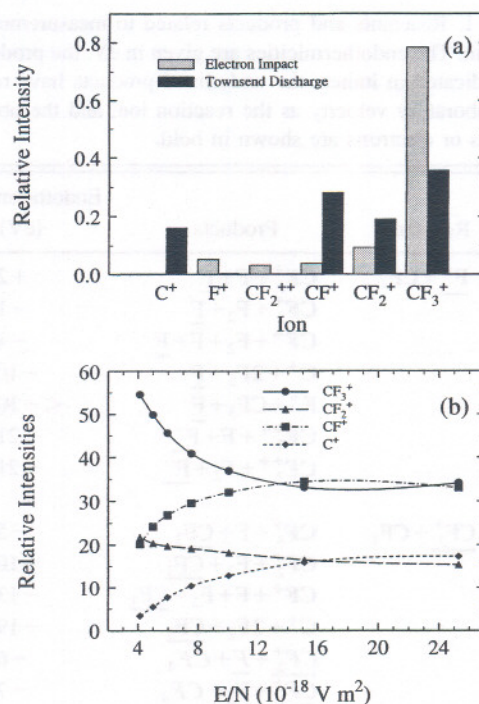


FIG. 5. (a) Comparison of standard electron-impact mass spectrum of CF_4 for 70 eV electrons, with the mass spectrum of positive ions sampled from a CF_4 Townsend discharge with $E/N = 11.4 \times 10^{-18} \text{ V m}^2$ (11.4 kTd). The two mass spectra are normalized to have equal total signals. (b) The relative intensities of the four dominant ions sampled from CF_4 Townsend discharges at various values of E/N .

(the two cannot be distinguished in the CID measurements), CF^+ , and CF_2^+ were found to have almost exactly the same energy-independent cross sections, each with a magnitude of $6 \pm 1 \text{ \AA}^2$. Again, no evidence could be found for the production of free electrons for these reactants.

3. $\text{F}^- + \text{CF}_4$

Cross sections for electron detachment for $\text{F}^- + \text{CF}_4$ are given in Fig. 4. Electron detachment begins at the electron affinity of F^- (3.4 eV) and increases rapidly with energy. The cross section is somewhat similar in magnitude and behavior to that reported for F^- impacting rare gas targets [19] and shows that electron detachment may be a significant contributor to the population of chemically active fluorine, an important radical in plasma etching processes.

B. Townsend discharge experiments

Figure 5(a) shows an energy-integrated mass spectrum of positive ions striking the cathode of a Townsend discharge in CF_4 (black bars), as measured by the mass spectrometer-energy analyzer system. The F^+ ion exhibited a signal intensity near the detection limit of the instrument at all E/N , and CF_2^{++} was never observed. F^- and CF_3^- were the only negative ions detected. Both exhibited weak signals, as compared to the positive ions, with CF_3^- consistently exhibiting a flux nearly 10 times smaller than that for F^- . For comparison, the standard 70-eV electron-impact mass spectrum [20] for CF_4 is also shown (gray bars) in Fig. 5(a).

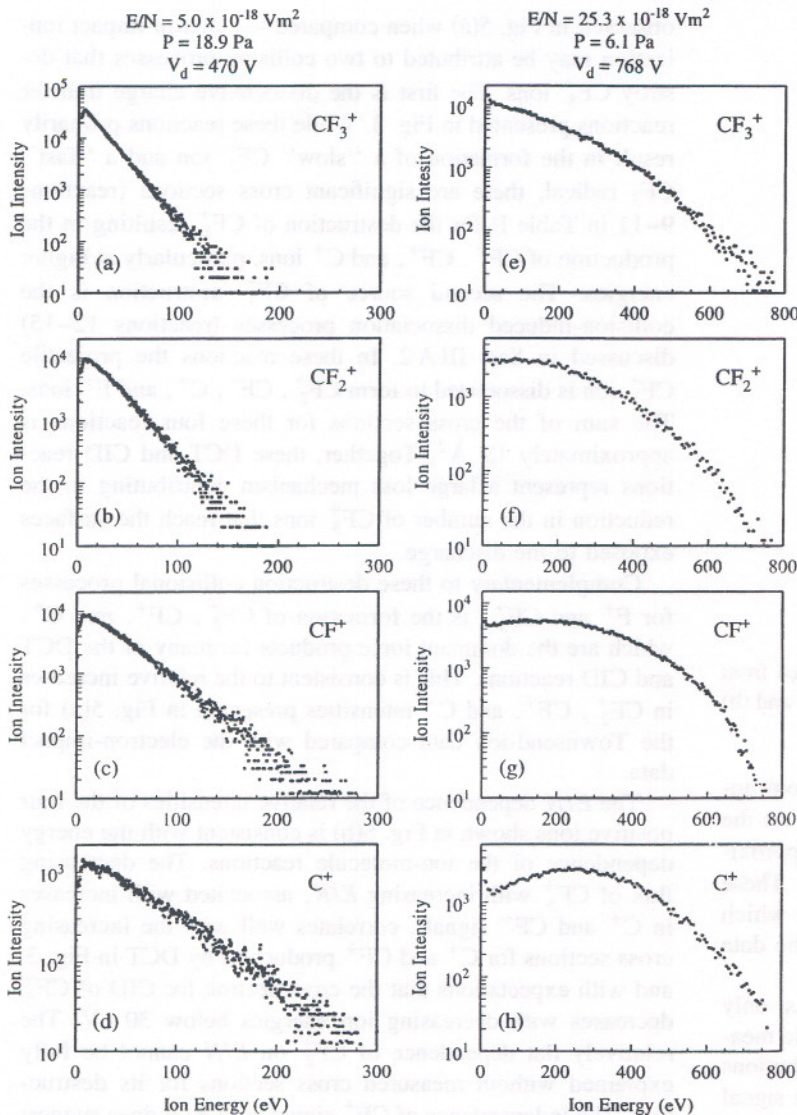


FIG. 6. Ion-flux energy distributions for positive ions sampled from CF_4 Townsend discharges with $E/N = 5.0 \times 10^{-18} \text{ V m}^2$ and $25.3 \times 10^{-18} \text{ V m}^2$ (5 and 25.3 kTd).

The actual energy distribution of electrons in the Townsend discharge is unknown (no calculations or measurements have been made at this high E/N), but it is expected to be non-Maxwellian with a high energy tail. It is therefore an oversimplification to assume that the 70-eV electron-impact mass spectrum is indicative of the positive ions formed by electron impact in the discharge. Even so, it is reasonable to assume that the differences between the two mass spectra in Fig. 5(a) may be partially attributed to the ion-conversion collisions that the ions experience as they travel through the discharge after having been formed by electron-impact ionization. Thus in general one can surmise from Fig. 5(a) that ion-molecule reactions exist that destroy CF_3^+ and F^+ ions, while creating C^+ , CF^+ , and CF_2^+ ions.

The relative intensities of the four dominant ions were observed to vary with the value of E/N in the discharge. This is shown in Fig. 5(b), where the intensity of CF_3^+ is observed to decrease with increasing E/N , the intensities of C^+ and CF^+ increase with increasing E/N , and the intensity of CF_2^+ is nearly independent of E/N .

Figure 6 shows the energy distributions for the four dominant positive ions detected from two CF_4 Townsend discharges with E/N values near the extremes of the range in-

vestigated here. The F^+ ion signal intensities were too weak to allow the measurement of energy distributions. At $5 \times 10^{-18} \text{ V m}^2$, the distribution for each ion exhibits a nearly linear decay with increasing energy on the semilog plots. This has been shown to be indicative of equilibrium motion of ions through the discharge [11,12], i.e., each ion experiences many collisions before striking the cathode. Interestingly, the maximum ion energies of the distributions, and the corresponding mean energies, increase with decreasing mass, indicating that the magnitude of cross sections for collisions resulting in energy loss are smaller for the smaller ions.

At the higher E/N value ($25.3 \times 10^{-18} \text{ V m}^2$), the distributions exhibit significant curvature, and the maximum ion energies are equivalent to the voltage drop between the electrodes (768 V). Both of these observations indicate a lack of equilibrium conditions for the ions, i.e., the ions experience too few collisions to exhibit an energy distribution characterized solely by E/N . In fact, some of the ions travel across the electrode gap without experiencing any significant energy loss. Again the mean energies of the distributions increase with decreasing mass of the ion, which is a trend that was observed at all values of E/N studied here.

By integrating the ion-flux energy distributions, the mean energies of the ions were calculated. The mean energies at

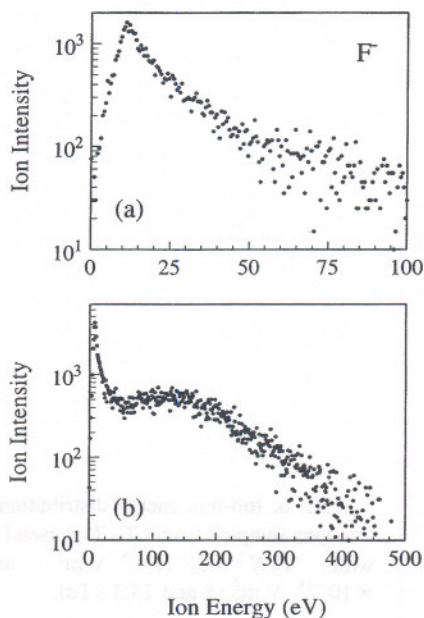


FIG. 7. Ion-flux energy distributions for F^- ions sampled from CF_4 Townsend discharges with (a) $E/N=4.0 \times 10^{-18} \text{ V m}^2$ and (b) $E/N=16.8 \times 10^{-18} \text{ V m}^2$.

low $E/N=4 \times 10^{-18} \text{ V m}^2$ are observed to range from approximately 20 eV for CF_3^+ to nearly 40 eV for C^+ . At the highest value of E/N , the mean energies range from approximately 150 eV for CF_3^+ to nearly 250 eV for C^+ . These values provide an indication of the ion energies for which ion-molecule cross sections are needed to interpret the data from these types of discharges.

For the negative ions detected from the discharges, only F^- exhibited sufficient signal intensity to allow reliable measurements of ion-flux energy distributions. The distributions for F^- at two values of E/N are shown in Fig. 7. The signal intensities are weak compared to positive ion intensities, and the maximum ion energies are also lower than observed for positive ions at the same E/N . The mean ion energies for F^- range from 25 eV at $4 \times 10^{-18} \text{ V m}^2$ to 110 eV at $17 \times 10^{-18} \text{ V m}^2$.

IV. DISCUSSION

Some of the Townsend discharge data presented in Figs. 5–7 may be interpreted in light of the cross section data presented in Figs. 2–4 and the discussion in Sec. III A. The nearly total lack of F^+ flux in the Townsend discharges is attributable to the dissociative charge transfer reactions shown in Fig. 2. Only a small portion of the total cross section for DCT results in the formation of a new F^+ ion (reaction 5 in Table I). The remaining collision pathways result in the destruction of F^+ and the formation of a different ionic species, thus nearly eliminating F^+ from the discharge before it can reach the cathode. Interestingly, from the cross section data in Fig. 2, one would expect a substantial CF_2^{++} signal to be observed from the Townsend discharge. However, no CF_2^{++} ion flux was detected, perhaps indicating that a large collisional destruction process, such as charge transfer, also exists for CF_2^{++} .

Similarly, the relatively lower intensity of the CF_3^+ ion

observed in Fig. 5(a) when compared to electron-impact ionization may be attributed to two collision processes that destroy CF_3^+ ions. The first is the dissociative charge transfer reactions presented in Fig. 3. While these reactions primarily result in the formation of a “slow” CF_3^+ ion and a “fast” CF_3 radical, there are significant cross sections (reactions 9–11 in Table I) for the destruction of CF_3^+ resulting in the production of CF_2^+ , CF^+ , and C^+ ions, particularly at higher energies. The second source of CF_3^+ destruction is the collision-induced dissociation processes (reactions 12–15) discussed in Sec. III A 2. In these reactions the projectile CF_3^+ ion is dissociated to form CF_2^+ , CF^+ , C^+ , and F^+ ions. The sum of the cross sections for these four reactions is approximately 18 \AA^2 . Together, these DCT and CID reactions represent a large loss mechanism contributing to the reduction in the number of CF_3^+ ions that reach the surfaces exposed to the discharge.

Complementary to these destruction collisional processes for F^+ and CF_3^+ , is the formation of CF_2^+ , CF^+ , and C^+ , which are the dominant ionic products for many of the DCT and CID reactions. This is consistent to the relative increases in CF_2^+ , CF^+ , and C^+ intensities presented in Fig. 5(a) for the Townsend-ion data compared with the electron-impact data.

The E/N dependence of the relative intensities of the four positive ions shown in Fig. 5(b) is consistent with the energy dependence of the ion-molecule reactions. The decreasing flux of CF_3^+ with increasing E/N , associated with increases in C^+ and CF^+ signals, correlates well with the increasing cross sections for C^+ and CF^+ production by DCT in Fig. 3, and with expectations that the cross section for CID of CF_3^+ decreases with decreasing ion energies below 30 eV. The relatively flat dependence of CF_2^+ on E/N cannot be fully explained without measured cross sections for its destruction. The independence of CF_2^+ signal with E/N does suggest that some significant destruction processes exist that would compete with the significant production processes for CF_2^+ measured here in reactions 2, 9, and 12.

The large cross section measured for the production of “slow” CF_3^+ ions by DCT from CF_3^+ (reaction 8 and Fig. 3) explains the relatively low energies of the CF_3^+ ions shown in Fig. 6, as compared to the other positive ions. It has been shown for other gases, that such charge transfer reactions significantly reduce the mean energies of that ion in the discharge [11,12]. Based upon the observed trend in ion energies with changing mass that is evident in Fig. 6, similar DCT cross sections would be expected for CF_2^+ , CF^+ , and C^+ , although the magnitudes would be somewhat related to the mass of each ion.

Dissociative electron attachment to CF_4 is weak [15], so F^- intensities are expected to be weaker than positive ion intensities in the CF_4 Townsend discharge. Additionally, the significant cross section for collisional electron detachment for F^- (reaction 16) at the ion energies exhibited by the distributions shown in Fig. 7 will further reduce the amount of F^- detected at the electrode. The increasing cross section for collisional detachment with increasing energy (Fig. 4) explains the relatively low ion energies observed for F^- compared to the smaller positive ions.

Because of the relatively high pressures and long transport distances existing in the Townsend discharges, the ion-molecule reactions measured and discussed here significantly influence the energy and species distributions for ions striking the surfaces exposed to the discharge. The influence of these reactions will be less for low pressure discharges with small sheaths where the ions experience far fewer high energy ion-molecule collisions. For example, ion-flux data taken in an inductively coupled, CF_4 plasma [21] exhibit narrow ion-energy distributions and relative ion fluxes similar to the 70-eV mass spectrum shown in Fig. 5(a), thus indicating minimal ion-molecule collisions as the ions are accelerated toward the grounded electrode.

Other discharges that are commonly used for plasma processing application possess characteristics that would suggest a potentially significant role of ion-molecule reactions in determining the composition and energy of the ion flux. For example, capacitively coupled plasmas commonly operate at pressures ranging from 1.3 to 133 Pa (10 to 1000 mTorr) and exhibit sheath widths larger than a millimeter. At these pressures the mean free path of an ion can be smaller than the sheath width, and depending upon the reactor design, the ions can have energies exceeding 100 eV. [22]

Ion intensity and energy distributions for capacitively coupled CF_4 discharges reported by Janes [23] showed that intensities of CF^+ and CF_2^+ ions increased with increasing gas pressure. These observations are in agreement with the cross section measurements presented here. Janes attempted to identify possible ion-molecule reactions to explain his observations, but acknowledged the need for energy dependent cross sections for a detailed analysis of the structures observed in the ion-energy distributions.

In a similar measurement for a CF_4 , capacitively coupled discharge, Snijkers *et al.* [24] concluded that a large number of chemical reactions take place within the sheath involving CF_x^+ ions and neutrals. From an analysis of their ion-energy distributions, Snijkers *et al.* attempted to deduce the dominant ion-molecule reactions occurring within the sheath. While their analysis resulted in the identification of some of the systems measured here, it was not possible from the available data to ascertain all of the important reactions. The use of the present cross sections allows for some additional

analysis of their results. For example, Snijkers *et al.* concluded that CF_2^+ ions were produced in the sheath primarily by the dissociation of CF_3^+ ions, which is supported by our cross section measurements for that reaction (reaction 12 in Table I). However, they did not consider the production of CF_2^+ from CID reactions such as reactions 2 and 9 shown in Figs. 2 and 3, respectively. Similarly, the production of CF_3^+ ions in the sheath are attributed primarily to CID reactions of CF_3^+ ions with CF_4 (reaction 8), while a CID reaction involving F^+ (reaction 1) may also contribute. Finally, the production of F^+ in the sheath was attributed primarily to symmetric charge-exchange collisions with F radicals. Equally likely production mechanisms include the CID reaction of CF_3^+ striking CF_4 to form F^+ (reaction 14) and the DCT reaction of F^+ striking CF_4 to form F^+ (reaction 5).

V. CONCLUSIONS

We have presented cross sections for ion-molecule reactions that are typically found in many CF_4 discharges. These reactions include dissociative charge transfer for F^+ and CF_3^+ , collisional induced dissociation for CF_3^+ , and collisional electron detachment for F^- . Also presented were measurements of kinetic energies and relative intensities of ions sampled from dc Townsend discharges. Analysis of the cross sections presented at the beginning of the paper allowed a general interpretation of the characteristics of the ion flux measured at the electrodes of the Townsend discharge. This suggests that the processes for which cross sections were determined represent the primary ion-molecule reactions occurring within the discharge. However, a complete assessment of the ion production and transport within the discharge would require a more complete measurement of cross sections, including CID and DCT cross sections for the less abundant ions, such as C^+ , CF^+ , CF_2^+ , and CF_2^{++} .

ACKNOWLEDGMENT

The work at W&M was supported by the Division of Chemical Sciences, Office of Basic Energy Sciences, U. S. Department of Energy.

- [1] *Data Needs for Modeling and Simulation of Plasma Processing*, National Research Council Report (National Academy Press, Washington, DC, 1996).
- [2] M. Meyyappan, D. Bose, D. Hash, H. Hwang, and T. R. Govindan, *Proc. Electrochem. Soc.* **98-4**, 43 (1998).
- [3] T. J. Sommerer and M. J. Kushner, *J. Appl. Phys.* **71**, 1654 (1992).
- [4] P. L. G. Ventzek, T. J. Sommerer, R. J. Hoekstra, and M. J. Kusher, *Appl. Phys. Lett.* **63**, 605 (1993).
- [5] P. L. G. Ventzek, R. J. Hoekstra, and M. J. Kusher, *J. Vac. Sci. Technol. B* **12**, 461 (1994).
- [6] M. Meyyappan and T. R. Govindan, *J. Appl. Phys.* **80**, 1345 (1996).
- [7] T. Simko, V. Martisovits, J. Bretagne, and G. Gousset, *Phys. Rev. E* **56**, 5908 (1997).
- [8] B. L. Peko, R. L. Champion, and Y. Wang, *J. Chem. Phys.* **104**, 6149 (1996).
- [9] B. L. Peko and R. L. Champion, *J. Chem. Phys.* **107**, 1156 (1997).
- [10] E. R. Fisher, M. E. Weber, and P. B. Armentrout, *J. Chem. Phys.* **92**, 2296 (1990).
- [11] M. V. V. S. Rao, R. J. Van Brunt, and J. K. Olthoff, *Phys. Rev. E* **54**, 5641 (1996).
- [12] M. V. V. S. Rao, R. J. Van Brunt, and J. K. Olthoff, *Phys. Rev. E* **59**, 4565 (1999).
- [13] J. K. Olthoff, R. J. Van Brunt, S. B. Radovanov, J. A. Rees, and R. Surowiec, *J. Appl. Phys.* **75**, 115 (1994).
- [14] H. R. Skullerud and S. Holmstrom, *J. Phys. D* **18**, 2375 (1985).
- [15] L. G. Christophorou, J. K. Olthoff, and M. V. V. S. Rao, *J. Phys. Chem. Ref. Data* **25**, 1341 (1996).

